Journal of Solid State Chemistry 184 (2011) 2595–2600

Contents lists available at ScienceDirect

Journal of Solid State Chemistry

journal homepage: www.elsevier.com/locate/jssc

The complex synthesis and solid state chemistry of ceria–lanthana solid solutions prepared via a hexamethylenetetramine precipitation

P.G. Fleming [a,b,*], J.D. Holmes [a,b,c,d], D.J. Otway [a,c], M.A. Morris [a,b,c,d]

[a] Department of Chemistry, University College Cork, Cork, Ireland
[b] Environmental Research Institute, University College Cork, Cork, Ireland
[c] Tyndall National Institute, Lee Maltings, Cork, Ireland
[d] CRANN, Trinity College Dublin, Dublin, Ireland

ARTICLE INFO

Article history:
Received 8 March 2011
Received in revised form
29 June 2011
Accepted 6 July 2011
Available online 22 July 2011

Keywords:
Solid solutions
Ceria–lanthana
Hexamethylenetetramine
Cubic lanthana

ABSTRACT

Mixed oxide solid solutions are becoming ever more commercially important across a range of applications. However, their synthesis can be problematical. Here, we show that ceria–lanthana solid solutions can be readily prepared via simple precipitation using hexamethylenetetramine. However, the solution chemistry can be complex, which results in the precipitated particles having a complex structure and morphology. Great care must be taken in both the synthesis and characterisation to quantify the complexity of the product. Even very high heat treatments were not able to produce highly homogeneous materials and X-ray diffractions reveals the non-equilibrium form of particles prepared in this way. Unexpected crystal structures are revealed including a new metastable cubic La_2O_3 phase.
© 2011 Elsevier Inc. All rights reserved.

1. Introduction

Cerium dioxide (CeO_2), ceria, and it's solid solutions hold significant importance in oxidative/reductive catalysis [1], as an electrolyte material in intermediate temperature fuel cells [2], as polishing materials [3] and gas sensors [4]. The production of ultrafine nanoparticulate CeO_2 and various solid solutions by the homogeneous precipitation using hexamethylenetetramine (HMT) has attracted much attention [5–9]. These HMT techniques offer advantages over conventional precipitation because the growth of the precipitate occurs very slowly and is thought to produce very homogeneous particles with a very regular distribution of cations. The fine particles that result from this synthesis method have increased sinterability making them attractive in the production of solid electrolytes [10]. Little information, however, is available on the homogeneous precipitation of ceria–lanthana solid solutions. Here, we present our findings on the synthesis of ceria–lanthana solid solutions by homogeneous precipitation using HMT. It is shown that great care in synthesis is required if the methodology is to be used for production of homogeneous particles and the products can be structurally highly complex with unexpected composition and component distributions.

2. Experimental

Homogeneous precipitation reactions were carried out according to Chen and Chen [5] using mixtures of cerium and lanthanum nitrate solutions. The reactants, cerium and lanthanum nitrate and hexamethylenetetramine (HMT) were all sourced from Sigma Aldrich. Equivalent volumes of 0.5 M HMT and 0.0375 M mixed metal nitrate solutions were mixed and stirred overnight (a nucleation phase designed to give small and regular particle sizes) before being heated to 90 °C for 2 h (growth phase). The solutions were then allowed to cool to room temperature before the precipitate was collected by centrifuging at 10,000 rpm for 30 min. The collected precipitate was washed three times by re-dispersion in de-ionised water followed by re-collection by centrifuging as before. The samples prepared were: CLO5, CLO10, CLO15, CLO20, CLO30, CLO40, CLO50, CLO60, CLO70, CLO80, CLO85, CLO90, and CLO95, where the numeric value is the target mole% of lanthanum (according to solution concentrations). Small amounts of ZrO_2 were added to the samples (after calcination), which were then re-ground, to act as an internal reference for accurate determination of lattice spacing. By comparison to samples prepared without the reference zirconia it was proven that this had no active role in any solid state chemistry. Pure CeO_2 and La_2O_3 were also synthesised as references. The retrieved precipitates were dried overnight at 100 °C and further calcined to 300, 500, 600, 700, 800, 900, 1000, 1100, 1200, and 1300 °C at a heating rate of 10 °C min^{-1}. The powders were kept at temperature for 2 h before

* Corresponding author at: Department of Chemistry, University College Cork, Cork, Ireland.
E-mail address: Peter.Fleming@ucc.ie (P.G. Fleming).

0022-4596/$ - see front matter © 2011 Elsevier Inc. All rights reserved.
doi:10.1016/j.jssc.2011.07.004

being cooled back to room temperature at a rate of 10 °C min^{-1}. Powder X-ray diffraction (PXRD) was performed on a Panalytical MPD instrument using a Xcelerator detector and a Cu $K\alpha$ radiation source at a working power of 45 kV and 40 mA. Lattice parameters were calculated using the peak positions of the <2 0 0>, <2 2 0> and <3 1 1> reflections. These data were then averaged to give the lattice parameter of each sample. Total reflectance X-ray fluorescence spectroscopy (TXRF) was performed to obtain the actual Ce:La concentration of the samples using a Bruker S2 Picofox instrument. Semi-quantitative analysis was used to determine cation concentrations and these were verified against several physical mixtures, which were within 2 mol% of the expected composition. X-ray photoelectron spectroscopy (XPS) was carried out on a VSW Atomtech system (Al $K\alpha$ radiation at 50 eV pass energy) and Raman analysis on an Invia Renishaw instrument.

3. Results and discussions

The PXRD spectra obtained for the samples after calcination at 500 °C are shown in Fig. 1. A single cubic fluorite phase is seen for all samples until a nominal concentration of 70 mol% (CLO70) is reached when additional features are observed at what is the effective solubility limit. These additional features are discussed further below. The data from CL05 to CL070 shows a single fluorite-like phase and the reflection positions indicate a continuous expansion of the lattice with increasing La^{3+} content caused by the larger size of La^{3+} cation compared to the host Ce^{4+} cation [11]. Crystallite size was calculated using the Scherrer equation from the obtained FWHM from the <2 0 0> reflection. The calculated size for CeO_2 after calcination at 500 °C was 13.9 nm, this value gradually decreased with increasing La^{3+} concentration to a value of 10.9 nm for CLO60. Peaks due to presence of the ZrO_2 reference were the only other features observed. The observed solubility limit is in agreement with previous reports for the same system [12–14]. It might be concluded from these data that homogeneous solid-solutions of controlled and predictable composition are produced. This was not seen to be the case on careful study. Raman spectroscopy was carried out to investigate the homogeneity of the samples; results are shown in Fig. 2. Each spectrum is an overlay of 4 different scans taken from different areas of a powder sample. For samples CLO5 to CLO60 the spectra are dominated by a large intense peak and there is little variation form the point-to-point analysis suggesting the samples were reasonably homogeneous. However, for CLO70 and higher composition samples the data shows multiple peaks with little consistency from point-to-point analysis. Of the secondary features, the most notably is an −OH feature at 3600 cm^{-1}. We have previously found that the rate of hydroxylation of lanthanum oxide species is fast [15] and, therefore, the appearance of this hydroxyl feature may be an indication of the formation of secondary minor La_2O_3 phases (which are rapidly hydroxylated) which are not observable by PXRD. These results support PXRD that a lanthanum loading of around 60 mol% represents a solubility limit above which secondary phase formation occurs. Further, at these higher concentrations sample homogeneity is lost.

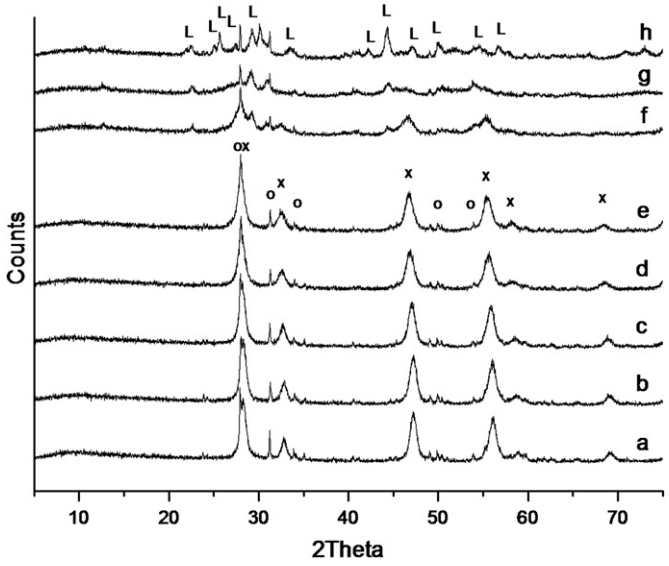

Fig. 1. XRD patterns obtained for (a) CeO_2, (b) CLO10, (c) CLO20, (d) CLO50, (e) CLO60, (f) CLO70, (g) CLO90 and (h) La_2O_3 after calcination at 500 °C for 2 h. X symbols correspond to the cubic fluorite phase JCPDS –34-394 and O symbols to the reference ZrO_2 and L corresponds to $La_2O_2CO_3$.

TXRF was carried out to confirm the lanthanide ratios, these results are shown in Table 1. In all samples below around a target composition of 90 mol% La, the measured lanthanum concentration was unexpectedly below that expected from the concentration of metal cations in the mixed solution used in preparation. Selected preparations were repeated for confirmation (also Table 1). These anomalies might be explained by complex solution chemistry. As outlined by Chen and Chen [5] these HMT synthesis methods represent a complex solution-solid series of equilibria between amine, hydroxyl anions, and the nucleating solid hydroxyl-phases. Allen et al. [16] carried out an in depth study of cerium ion solution chemistry during the particle growth of CeO_2 by HMT. They found that particle growth proceeds through a complicated mechanism where it was suggested that the Ce^{3+} cation formed cage like complexes with the tetradentate HMT ligand prior to hydrolysis. These complexes then formed a shell around nucleating particles indicating that they were an intermediary in particle growth. A more exact growth mechanism has yet to be detailed in the literature to our knowledge but from this information a model for the ceria–lanthana system may be proposed where ceria enrichment results from two different phenomena. Firstly, the smaller more acidic Ce^{3+} (or Ce^{4+} cations depending on conditions) forms more thermodynamically stable complexes with these chelating ligands than the larger more basic La^{3+} cation. This preferential Ce^{3+} complex formation would, therefore, result in Ce-HMT rich outer layer during particle growth and a lower total La^{3+} composition than that expected from the solution concentration. Secondly, and probably of greater importance, is the high solubility of $La(OH)_3$ (i.e. the precipitation product) in aqueous solution, which prevents precipitation [17]. As can be seen in Fig. 3, the enrichment in ceria in the samples is reduced as the preparations become La^{3+} rich. This is as expected because La^{3+} inclusion would be favoured as the solution concentration of Ce^{3+} reduces and the solution solubility limit of $La(OH)_3$ is exceeded. More detailed discussion is given below.

The most interesting observation from the PXRD data (see Fig. 1) was the appearance of a previously unreported cubic phase for CLO70 and samples prepared at higher concentrations. More explicit data is provided in Fig. 4, which shows the evolution of phase transformation as observed for CLO70 after calcination at different temperatures. At low temperatures (500 °C—Fig. 4a), two phases were observed namely monoclinic $La_2O_2CO_3$ (JCPDS—22-1127) and a broad fluorite structure (JCPDS—34–394). The presence of this oxycarbonate phase is consistent with evidence of $La(OH)_3$ in Raman because $La(OH)_3$ and $La_2O_2CO_3$ are the products of air exposure of La_2O_3 to ambient [15]. The oxycarbonate phase did not decompose to form hexagonal La_2O_3 at higher temperatures as usually observed in lanthanum only materials [15] but rather appears to form a cubic structure as indicated in Fig. 4b and c on heating to temperatures between 700 and 1000 °C. The position of the reflections is at much lower 2θ and, hence, larger

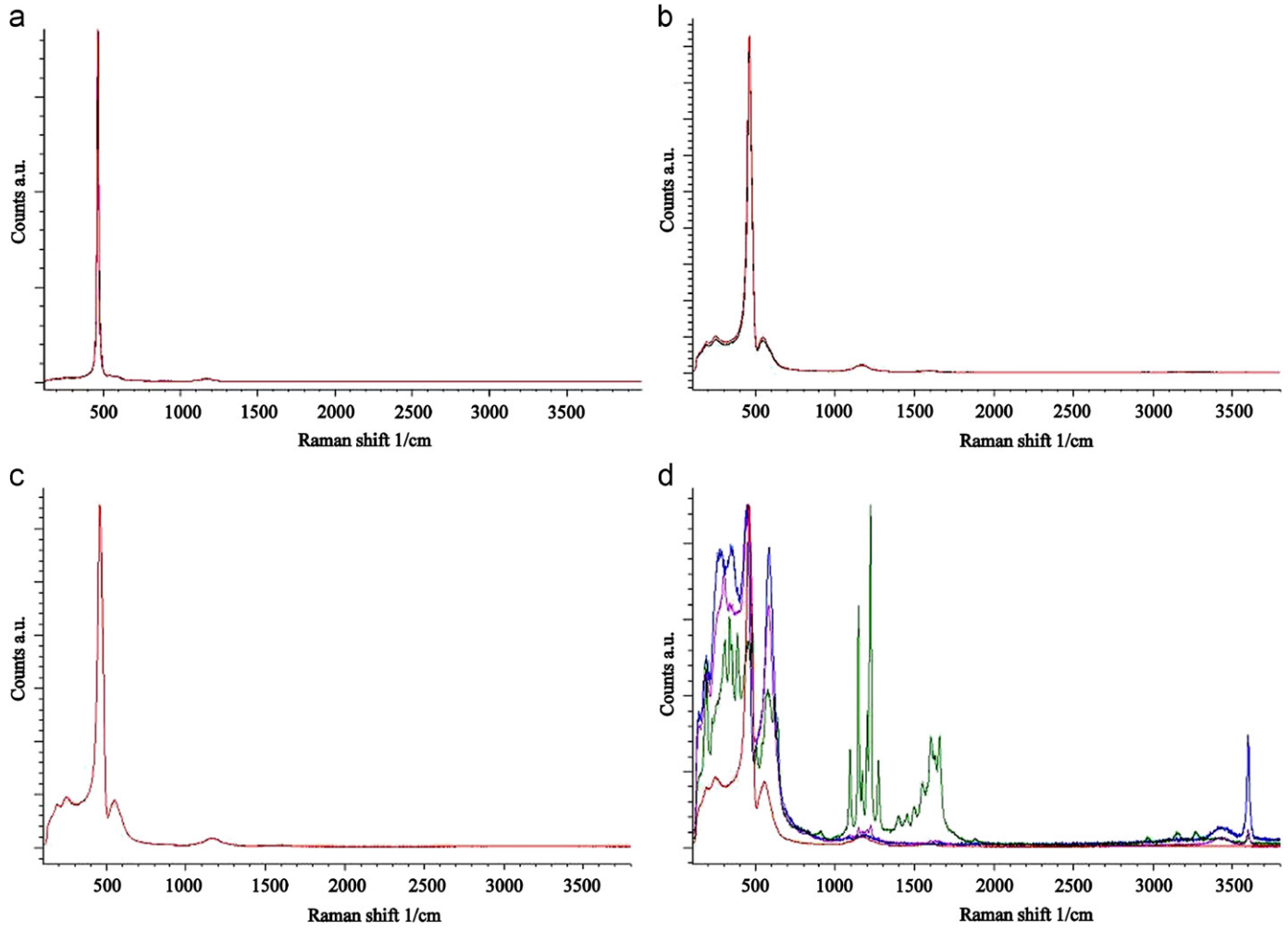

Fig. 2. Different area Raman spectra for (a) CLO15, (b) CLO50, (c) CLO60 and (d) CLO70.

Table 1
Target and observed compositions (mole%La) for the prepared samples.

Mole% La Target	Measured from prep 1	Measured from prep 2
0	0.2	0.1
5	1	1.7
10	4.2	2.9
12.5	–	3.9
15	4	6.4
17.5	–	6.6
20	7.7	6.2
30	10	10.7
40	13.5	–
50	17	19.6
60	23.5	–
70	51.3	–
80	57.3	–
85	73.3	–
90	83.4	–
95	93.5	–
100	96.4	–

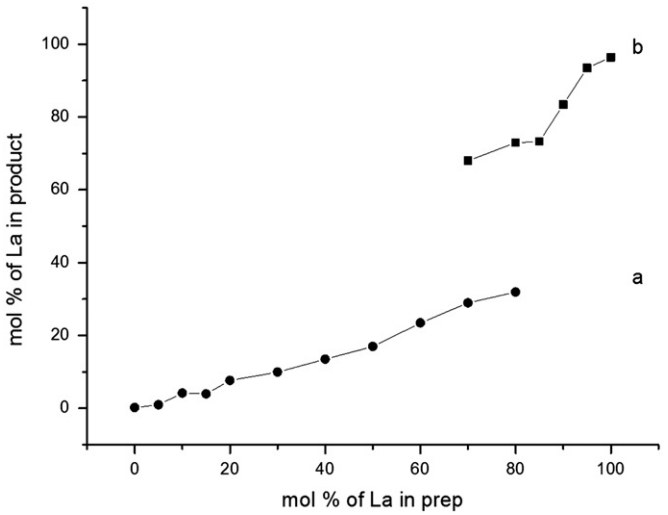

Fig. 3. Observed composition of La (mol%) compared to the theoretical mol% for (a) cubic fluorite phase and (b) La rich phases.

lattice spacing than expected for a solid solution of lanthana in ceria within the normal solubility limits [11] and can only be explained by a very high content lanthana phase. Pattern refinement is consistent with a cubic structure previously unreported in the literature to our knowledge. It is suggested that this is based on a defective fluorite structure. On very high temperature calcination (1300 °C) this cubic phase is transformed into a fluorite-like structure (Fig. 4d) resulting in a pattern that consisted of a two, well-resolved, cubic fluorite phases presumably containing different La^{3+} content. Similar observations were made for the CLO80 sample, except that ratio of intensities of the two solid solution fluorite phases (X_1 and X_2 in Fig. 4) seen after 1300 °C

calcination are different. As might be expected (since the lanthana content is higher), the lower 2θ reflections due to the X_1 phase are of proportionally greater intensity than the X_2 phase compared to that observed for the CLO70 phase. The Ce mole% was measured by XPS after calcination at 500, 700 and 1300 °C and was found to be 72, 55 and 29 mol%, respectively. Concentration estimates were based on 3*d* peak area ratios using standard peak fitting and sensitivities as described in a previous paper [18]. This is consistent with the formation of a Ce rich layer formed around the particles and at high temperature calcination, mass transport results in increased cation homogeneity within the particles.

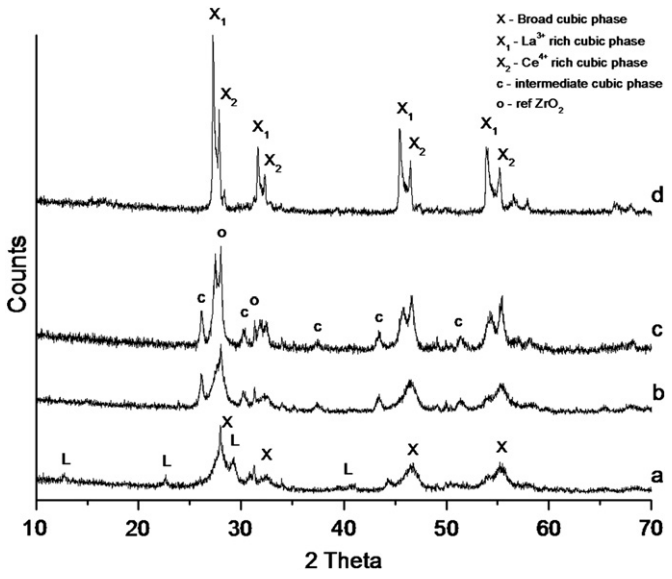

Fig. 4. Phase transformations of CLO70 upon calcination at (a) 500 °C (b) 700 °C (c) 1000 °C and (d) 1300 °C. L is a monoclinic $La_2O_2CO_3$, see text for further details.

A suggested mechanism for the creation of these dual fluorite phase particles is pictorially illustrated Fig. 5. During room temperature aging (Step 1, Fig. 5) the particles nucleate in a cerium rich stoichiometry (because of coordination and solution chemistry as discussed above) compared to the solution concentration of cations. At lower lanthanum concentrations, ceria enrichment is maintained because during the higher temperature growth phase the $La(OH)_3$ solubility is greater than the solution concentration. This is in agreement with solubility limits measured by Deberdt et al. [17], who found solubility limits, Log[La], of -3 at 40 °C, -4.5 at 60 °C and -6.5 at 90 °C at a pH of 7.5. As can be seen the solubility limit reduces significantly with increasing temperature and for CLO70 and CLO80 the concentration of La^{3+} in solution at 90 °C exceeds the solubility limit and this coupled to a reported reduction in complex formation at high temperatures [16] causes particle growth at a similar stoichiometry to the solution cation concentrations, which are now enriched in lanthanum because of preferential cerium precipitation at lower temperature (Step 2, Fig. 5). The particles continue

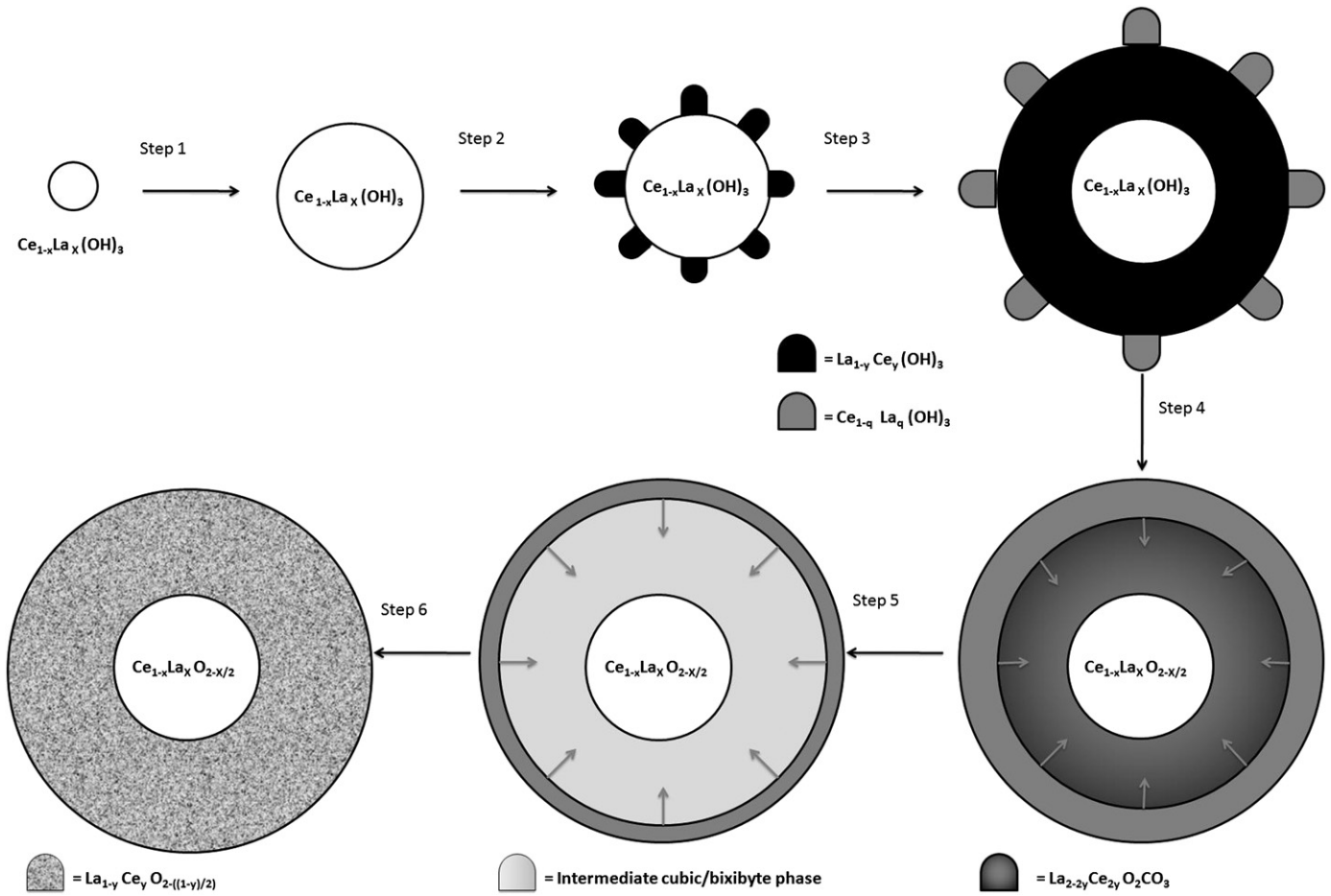

Fig. 5. Suggested mechanism for the formation of dual fluorite phase particles, where Step 1 corresponds to room temperature aging, Step 2 heating the solution to 90 °C, Step 3 cooling of the solution to room temperature, Step 4 calcination to 500 °C, Step 5 calcination to 700 °C and Step 6 calcination to 1300 °C. The terminology of e.g. $La_{1-x}Ce_x(OH)_3$ is used to indicate the formation of a mixed oxy-hydroxy participate rather than a definitive assignment of stoichiometry. Similarly, $La_{1-y}Ce_yO_{2-((1-y)/2)}$ only implies a mixed solid solution.

to grow at this stoichiometry until the solution in cooled to room temperature (Step 3, Fig. 5) when the increase in solubility of $La(OH)_3$ causes the preferential growth of a cerium rich outer layer similar to that seen in Step 1. In this way, the materials are essentially lanthanum deficient (compared to solution) and contain a cerium rich core and surface layer. This model allows the data presented in Fig. 4 to be explained. Upon calcination at 500 °C the La^{3+} rich layer (stoichiometry above that of the reported solubility limit of La^{3+} in CeO_2 [12]) forms the thermally (at this temperature) stable $La_2O_2CO_3$ phase by reaction with ambient CO_2. The cerium rich regions exhibit the expected cubic fluorite structure (Step 4, Fig. 5). Further calcination at 700 °C effects a decomposition of the lanthanum oxycarbonate phase. However, as opposed to the expected formation of hexagonal La_2O_3, a cubic-like structure is formed possibly via some form of epitaxy or structural templating mechanism. A reduction in the high cerium content of the outer layer is also observed indicating the migration and equilibration of the concentration of Ce^{4+} and La^{3+} between the two regions (Step 5, Fig. 5) as the system attempts to realise a thermodynamically stable solid-solution. Upon further calcination the Ce^{4+} concentration at the surface continues to decrease as the cubic-like structure, observed after Step 5 (Fig. 5), gradually transforms into a cubic fluorite structure due to cation diffusion. After calcination at 1300 °C the cubic lanthana phase is completely lost by ion mass transport and the particles now consist of two separated cubic fluorite patterns deriving from a core shell structure (Step 6 Fig. 5); an outer shell, which obtains a stoichiometry close to that of the reaction solution together with a cerium rich inner core.

At lower lanthana content, where an apparently simple (but La deficient) fluorite structure due to a solid solution of the cations is observed, the fluorite phase lattice parameter is linearly dependent on the La^{3+} concentration. However, plotting the lattice parameter over the entire content range (after 1300 °C) is difficult because of the mixed fluorite structures seen in CLO70 and CLO80 (high and low La^{3+} content). In order to calculate the content of each cubic phase observed for CLO70 and CLO80 (1300 °C) the measured TXRF concentration (i.e. the total concentration of La^{3+} in the sample) was weighted against the lattice parameter determined (since this is linearly depend on La^{3+}). The data are described in Fig. 6 as lattice parameter against actual La^{3+} content (determined by the weighted concentration). Also marked in the plot is a data point for the reported lattice parameter of cubic La_2O_3 (JCPDS 04–0856) which agrees well with the linear dependence reported here. It is interesting to note, for the 1300 °C calcined samples, that the calculated concentration of La in the outer La^{3+} rich shell (i.e. the fluorite phase at lowest 2θ angle) for CLO70 was 68 mol% while the La concentration measured by XPS for the same sample was 71 mol%. The agreement between the solution concentration, the surface concentration (as measured by XPS) and the bulk concentration (TXRF) of this outer layer La does suggest that the model proposed above for the complex structure of the as-synthesised materials is correct. It is probably that this equilibration of cation distribution derives from Ce^{4+} diffusion since these cations are smaller and more mobile in the fluorite lattice. CLO70 calcined at 1300 °C, after initial analysis, was re-calcined to 1300 °C under the same heating rates as described earlier and kept at temperature for 12 h. Once cooled XRD data confirmed the same intensity ratio of the two phases as observed for the same sample after calcination for 2 h indicating that thermodynamic equilibrium had been reached between the two phases at this temperature i.e. no further cation migration occurred. Our findings are, however, confined by our experimental limitations and the question of if further growth of the lanthanum rich phase at temperatures greater than 1300 °C remains to be answered.

It should be noted that the lanthanum concentrations in the outer La^{3+} shell for CLO70 and CLO80 using the methods described above is 68 and 73 mol%, respectively. These values exceed any previous reports of the La^{3+} solubility limit in the ceria fluorite structure [12–14]. This probably derives from the fact that the high concentrations result from reaction of the very La^{3+} rich cubic phase. This phase originates from the formation of the $La_2O_2CO_3$ structure, which when decomposed is 'directed' by the fluorite phases present to form a cubic phase. This is contentious argument because lanthana does not form stable cubic structures at this composition through precipitation synthesis. However, it has been shown that it can be directed into supersaturated structures, which show a very good stability to hydrolysis [19]. These results may have practical importance as La_2O_3 has been identified as one of several oxides that is suitable for the replacement of SiO_2 as a high k dielectric [20]. One of the practical problems, however, with the use of lanthana is its structural instability and tendency to hydrolyse. One of the approaches to overcome this is to produce cubic lanthana, which is more stable to ambient conditions and water in particular [19]. Fig. 7 shows the XRD pattern obtained for CLO70 (1300 °C) taken directly after calcination Fig. 7a) and one year after the initial

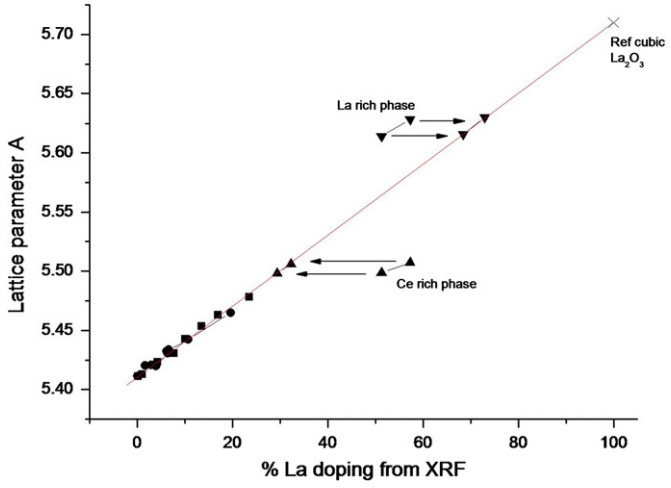

Fig. 6. Calculated lattice parameters observed for cubic fluorite phases against mol% La from TXRF.

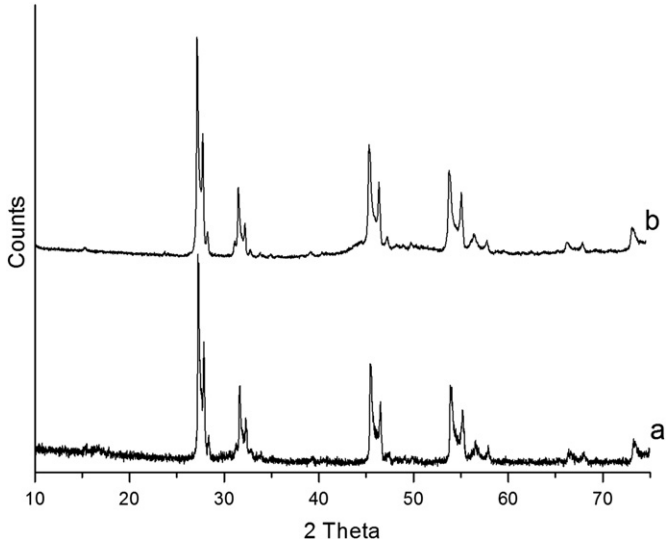

Fig. 7. XRD patterns for CLO70 (a) directly after calcination at 1300 °C and (b) the same sample 1 year later.

preparation Fig. 7b). The pattern remains the same without any major phase transformation, most notably to $La(OH)_3$, indicating the structure is very stable even on extended exposure to ambient conditions. It is suggested that the ambient stability of these supersaturated cubic lanthana phases merits further investigation as a means to increase the stability of lanthana.

4. Conclusions

This work shows that the preparation of ceria–lanthana solid solutions in particle form by simple chemical synthesis and precipitation can be more difficult than might be imagined. The product cation concentrations may not be as expected and, further, the products can have highly unusual core-shell structures with a highly inhomogeneous concentration of metal cations even after extended heating at high temperatures. In particular, it was found that at low lanthanide concentration HMT is an unsuitable precursor for the homogeneous precipitation of ceria–lanthana solid solutions. In the synthesis reaction during room temperature aging, cerium rich growth occurs and is suggested that this is caused by a thermodynamic preference for Ce^{3+} to complex with HMT [16] together with the solubility of $La(OH)_3$ in these conditions. Following calcination secondary crystallographic phases (besides that expected of a simple solid-solution) were observed above a critical lanthanum concentration. These secondary phases contain high lanthanum concentrations and at lower calcination temperatures are revealed by the appearance of a $La_2O_2CO_3$ phase. However, upon calcination at high temperatures the thermal decomposition of this oxycarbonate phase results in a previously unobserved cubic fluorite phase which proved very stable over time (>1 year). The formation of this metastable cubic La_2O_3 phase is thought to result from the structurally directing (i.e. templating) nature of cubic fluorite phases on La_2O_3 formation.

References

[1] A. Trovarelli, Catal. Rev. Sci. Eng. 38 (1996) 439–520.
[2] B.C.H. Steele, High Conductivity Soild Ionic Conductors, World Scientific, 1989.
[3] C.A. Coutinho, S.R. Mudhivarthi, A. Kumar, V.K. Gupta, Appl. Surf. Sci. 255 (2008) 3090–3096.
[4] P. Jasinski, T. Suzuki, H.U. Anderson, Sensors Actuators B—Chem. 95 (2003) 73–77.
[5] P.L. Chen, I.W. Chen, J. Am. Ceram. Soc. 76 (1993) 1577–1583.
[6] E.C.C. Souza, E.N.S. Muccillo, J. Alloy. Compds. 473 (2009) 560–566.
[7] T.C. Rojas, M. Ocana, Scr. Mater. 46 (2002) 655–660.
[8] J. Markmann, A. Tschope, R. Birringer, Acta Mater. 50 (2002) 1433–1440.
[9] A.I.Y. Tok, S.W. Du, F.Y.C. Boey, W.K. Chong, Mater. Sci. Eng. A—Struct. Mater. Prop. Microstruct. Process 466 (2007) 223–229.
[10] J.P. Liang, Q.S. Zhu, Z.H. Xie, W.L. Huang, C.Q. Hu, J. Power Sources 194 (2009) 640–645.
[11] K.M. Ryan, J.P. McGrath, R.A. Farrell, W.M. O'Neill, C.J. Barnes, M.A. Morris, J. Phys.—Condes. Matter 15 (2003) L49–L58.
[12] B.C. Morris, W.R. Flavell, W.C. Mackrodt, M.A. Morris, J. Mater. Chem. 3 (1993) 1007–1013.
[13] D.J.M. Bevan, J. Kordis, J. Inorganic Nucl. Chem. 26 (1964) 1509–1523.
[14] D.J.M.B.a.E. Summerville, Handbook on the Physics and Chemistry of Rare Earths (1979).
[15] P. Fleming, R.A. Farrell, J.D. Holmes, M.A. Morris, J. Am. Ceram. Soc. 93 (2010) 1187–1194.
[16] A.J. Allen, V.A. Hackley, P.R. Jemian, J. Ilavsky, J.M. Raitano, S.W. Chan, J. Appl. Crystallogr. 41 (2008) 918–929.
[17] S. Deberdt, S. Castet, J.L. Dandurand, J.C. Harrichoury, I. Louiset, Chem. Geol. 151 (1998) 349–372.
[18] P. Fleming, S. Ramirez, J.D. Holmes, M.A. Morris, Chem. Phys. Lett. 509 (2011) 51–57.
[19] M. Nieminen, M. Putkonen, L. Niinisto, Appl. Surf. Sci. 174 (2001) 155–165.
[20] A.C. Jones, H.C. Aspinall, R.R. Chalker, R.J. Potter, K. Kukli, A. Rahtu, M. Ritala, M. Leskela, Mater. Sci. Eng. B—Solid State Mater. Adv. Technol. 118 (2005) 97–104.